Interactions in Noncovalent PAMAM/TMPyP Systems Studied by Fluorescence Spectroscopy

Pedro M. R. Paulo* and Sílvia M. B. Costa

Centro de Química Estrutural, Complexo 1, Instituto Superior Técnico, Av. Rovisco Pais, 1049-001 Lisboa, Portugal

Received: February 21, 2005; In Final Form: April 22, 2005

Steady-state absorption and emission spectroscopy and time-resolved fluorescence measurements were employed in the study of *meso*-tetrakis(4-*N*-methylpyridinium)porphine (TMPyP) interactions with half-generation carboxyl-terminated poly(amidoamine) (PAMAM) dendrimers in water. TMPyP experiences a less polar environment and a strong fluorescence quenching effect upon dendrimer association. The tertiary amine functional groups in PAMAM dendrimers are likely to be responsible for the fluorescence quenching of TMPyP through an electron-transfer mechanism. The Stern−Volmer plots achieve a plateau at high dendrimer concentrations that was attributed to full porphyrin−dendrimer association, and an average fluorescence quantum yield of 15−20% relative to aqueous TMPyP was estimated. The association constant for the 1:1 complex with generation 2.5 at dendrimer−porphyrin ratio D/P = 1 is 5.75×10^7 M^{-1}, indicating a strong binding affinity. The dissociation of the complex with increasing ionic strength reinforces the role of electrostatic forces in porphyrin−dendrimer association. Comparison of Stern−Volmer plots obtained from quantum yields or lifetimes showed the importance of a static effect in these systems. The fluorescence decays of the porphyrin−dendrimer complex were fitted with a dispersed kinetics model. At intermediate dendrimer−porphyrin ratios (D/P $\approx$ 1), diffusional quenching processes between free porphyrin and dendrimer were modeled with the Sano−Tachiya pair survival probability equation. Transient diffusional effects were dismissed as a possible explanation for the static effect detected.

1. Introduction

Since the appearance of dendrimers in the early 1980s a great deal of attention has been devoted to this special class of polymers from diverse research fields.[1] The highly branched and regular structure of these macromolecules, that chemically reproduce well-known fractal topologies, has been mostly responsible for such interest. Dendrimers are built from a central unit or core, around which successive layers of repeating units or monomers are covalently attached to the terminal groups of the previous layer. These layers are usually termed generations and are numbered from the dendrimer's core to its periphery. The connecting multiplicity of the branching points is usually 2 or 3, which gives rise to a geometric growth of the dendrimer's mass with each generation. Eventually, above a certain generation, the stereochemical restraints prevent the growing of such structures.[2]

Studies on the interaction of dendrimers with small probe molecules have been carried out, exploiting hydrogen bonding[3] and the hydrophobic[4] and electrostatic effects.[5,6] In this context, porphyrins have been extensively investigated in water, organic solvents, or different molecular organisates due to their structural similarity with molecules of biological relevance such as chlorophylls and hemoglobin.

There are various examples in the literature of dendrimers functionalized with porphyrin units either in the core[7] or in terminal positions,[8] but only few studies deal with the noncovalent interactions of porphyrins with dendrimers.[9]

In a previous study, we focused on systems comprising anionic *meso*-tetrakis(4-sulfonatophenyl)porphyrin (TSPP) and oppositely charged full-generation dendrimers of the poly(amidoamine) family or PAMAMs.[6] These are among the first kind of dendrimers to be synthesized and are commercially available. In particular, the PAMAM dendrimers used have an ethylenediamine core and *N*-ethylpropanamide repeating units and are terminated with amine or carboxylate groups (Chart 1a). The branching points are tertiary amines, which present a pK_a in the range 3−6 and therefore are not protonated at neutral pH,[1a] but the terminal primary amines should be protonated. PAMAM dendrimers show a structural transition from an open and oblate conformation, at low generations, to a more compact and spherical one, above the third generation. This transition was predicted from molecular dynamics[10] and later experimentally confirmed.[5d,11]

Dendrimer-induced TSPP H-aggregates were identified in equilibrium with monomeric complexed TSPP in a nonbuffered medium, at similar molar concentrations of porphyrin and dendrimer, whereas, for a molar excess of TSPP, low-organized ("nonspecific") aggregates with broad absorption spectra and emission self-quenching were observed. At low pH, PAMAM dendrimers increase the J-type self-aggregation of TSPP and generation 4.0 is able to provide a more hydrophobic environment in comparison to generation 2.0.

meso-Tetrakis(4-*N*-methylpyridinium)porphine (TMPyP) is also a water-soluble porphyrin, for which the photophysical and electrochemical properties[12,13] and aggregation behavior[14] have been long investigated (Chart 1b). Studies on the interaction of tetracationic TMPyP with polyanion DNA have shown intercalative binding at G−C sites of the double helix, and possible applications for photodynamic therapy are being pursued.[15] For

* Corresponding author. E-mail: pcl41841@alfa.ist.utl.pt.

10.1021/jp050894f CCC: $30.25
Published on Web 07/06/2005

CHART 1

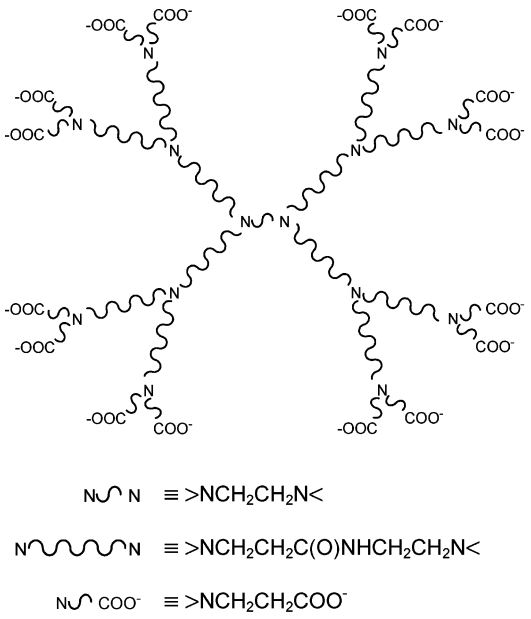

(a)

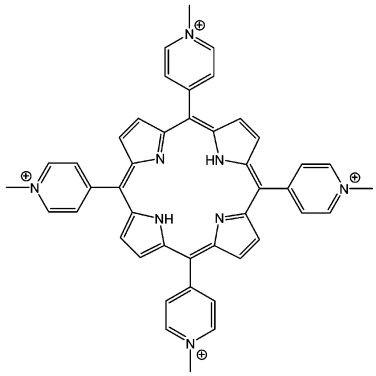

TMPyP

(b)

similar purposes, the antibacterial properties of TMPyP were studied and promising results were reported concerning its phototoxic activity.[16] TMPyP shows a great affinity for solid surfaces, and its adsorption at interfaces has been studied in diverse substrates, for example, in silica,[17] synthetic clays,[18] and Langmuir−Blodgett films.[19]

In the present work, the complexation of TMPyP with carboxyl-terminated PAMAM dendrimers was studied. The acids should be dissociated at neutral pH, resulting in a global negative charge for the dendrimers. Steady-state absorption and emission spectroscopy and time-resolved fluorescence measurements were employed to study the noncovalent interactions of TMPyP with oppositely charged half-generation PAMAM in water. The main phenomenology found in these assemblies is a strong fluorescence quenching effect, which was not detected with the negative TSPP analogue. Fluorescence decays of TMPyP/PAMAM reveal a large contribution of complex formation, in particular, at higher dendrimer concentrations. The modeling of the transient data was therefore carried out considering either only complex formation or the simultaneous occurrence of dynamic quenching between free porphyrin and dendrimer along with the complex formation.

2. Experimental Section

Materials. PAMAM dendrimers of generations 2.5 and 4.5 were supplied by Aldrich Chem. Co. as 10 and 5 wt % solutions in methanol, respectively. TMPyP was obtained from Dotite and was used without further purification. Triethylamine, *N*-ethylacetamide, and propionic acid were also from Aldrich and had a purity of at least 99%. Sodium chloride p.a. was acquired from Riedel-de Haën.

Sample Preparation. Stock solutions of PAMAM dendrimers in water were prepared by measuring adequate volumes of the methanolic solutions (as supplied) into volumetric flasks and evaporating the solvent under a gentle stream of N_2. Further removal of residual solvent was carried out overnight in a desiccator under vacuum. Reconstitution of the stock solutions was done with bidistilled water. Sample solutions were prepared from appropriate volumes of aqueous stock solutions of PAMAM and TMPyP to obtain the final dendrimer-to-porphyrin molar ratio (D/P ≡ [PAMAM]/[TMPyP]). Intermediate steps of agitation were applied to ensure complete homogenization of the samples before adding water to complete the volume.

The samples' aging was detected by measuring the same solutions at different time intervals after their preparation. Similar phenomena had already been reported in the literature for metal−ion complexes with PAMAM dendrimers studied by the electron paramagnetic resonance (EPR) technique.[4c,5b,c,20] For the systems studied here, the effects of porphyrin−dendrimer association are more pronounced shortly after sample preparation. It was also noticed that samples with a high D/P ratio age more slowly comparing, for instance, the D/P ratios of 1 and 10 in the systems with generation 2.5 PAMAMs. The aging effects observed in these systems show a gradual loss of porphyrin−dendrimer association over a period of hours to days. To avoid distortions in the results presented here, all measurements were performed within minutes after sample preparation and some care was taken to ensure that the samples' aging is not significant during that period.

Apparatus. Steady-state absorption spectra were acquired with a Jasco UV−vis V-560 spectrophotometer, and emission spectra were recorded with a Perkin-Elmer LS 50B spectrofluorimeter. Steady-state fluorescence anisotropy measurements were also performed with the latter equipment.

The time-correlated single-photon counting technique was employed to measure fluorescence decays using a commercial setup, Microtime 200. This instrument was adapted to measure samples in liquid solution with a cuvette by introducing an appropriate sample holder in the manual *XY* stage of the inverse microscope (Olympus IX 71). The measurements are performed in front-face geometry, and the backscattered light is attenuated through the use of appropriate filters. The excitation system consists of a pulse laser diode driver (PDL 800-B) equipped with a laser head for excitation at 400 nm, model LDH-P-C-400, which was used in the present work. The repetition rate of the pulsed laser can be controlled from 40 to 2.5 MHz in powers of $^1/_2$. The maximum output laser power for a repetition rate of 20 MHz (used here) is 0.8 mW, and its minimum pulse width is 54 ps. The detection system uses a photomultiplier tube from Picoquant (model PMA-182) with an instrument response time

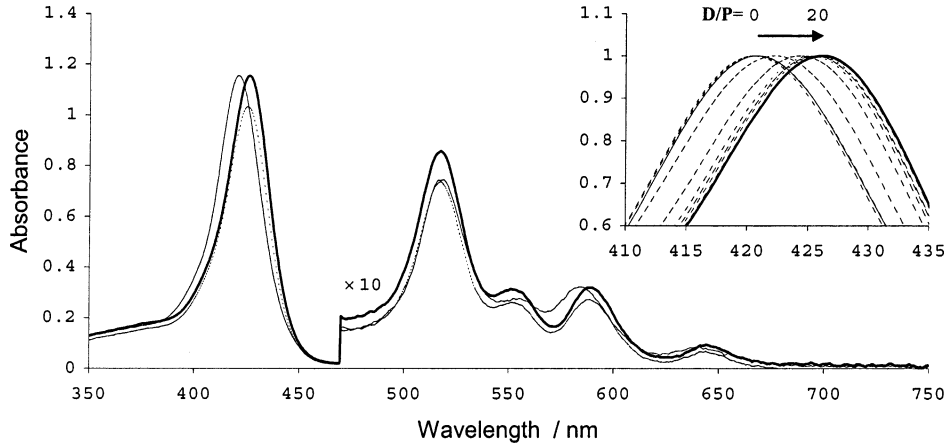

Figure 1. Absorption spectra of TMPyP in aqueous solution (D/P = 0, thin line) and with increasing concentration of PAMAM dendrimers of generation 2.5 (D/P = 1 and 10, dashed and solid lines, respectively). The inset shows the normalized absorption spectra in the peak of the Soret band for D/P ratios of 0, 0.2, 0.4, 0.5, 0.8, 1, 2, 3, 10, and 20.

below 250 ps. A band-pass filter from Omega Optical with a transmission window in the range 600−800 nm, that covers most of the emission spectra of aqueous TMPyP, was used to eliminate backscattered light. Data acquisition was performed with a PC equipped with a Timeharp 200 TCSPC board, also from Picoquant, which can record up to 4096 channels per range with a time increment smaller than 40 ps.

Data Analysis. Fluorescence decays were preliminarily analyzed with Fluofit software from Picoquant. This program was used to fit a multiexponential function to the experimental decays, through a nonlinear least-squares procedure based on the Marquadt−Levenberg algorithm[21] and combined with iterative reconvolution of the instrument response function.[22] The quality of the fittings was judged by the usual statistical criteria—in particular, the χ^2 value should have a value close to one—and also by visual inspection of the weighted residuals and autocorrelation function.

Fitting of the dispersed kinetics model to the fluorescence decays at high dendrimer concentrations was performed with an in-house-developed program[23] which also applies the Marquadt−Levenberg minimization algorithm combined with iterative reconvolution of the instrument response function. The integral appearing in the decay expression was numerically evaluated through Hermite integration.[24]

The numerical solution of the Sano−Tachiya equation, as presented further ahead, was obtained from the Crank−Nicholson finite difference method.[21] A variable time step was used to ensure better resolution at short times, starting with a step of 0.176 ps and increasing it by a factor of 4 every 500 steps to reach a final step of 11.5 ns and to span a time interval of about 7.69 μs with 4500 points. For the radial distance, a constant step of 0.1 Å was used to calculate approximately 4000 points. Such a tight mesh was required to obtain reasonable precision in the numerical derivations and integrations that are performed in calculating solutions for the global kinetics scheme (see Scheme 1). In particular, this matter affects the secondary production term, *J*, that involves several Laplace transforms. These were numerically evaluated with the trapezoidal rule for the direct transforms and through the Gaver−Stehfest[25] method for the inverse transform (using $N = 16$, according to ref 25b). Since the time/channel relation for the fluorescence decays is greater than the time step of the calculations, linear interpolation was used to match the time resolution of the decays. Convolution integrals were performed numerically with the trapezoidal rule.

3. Results

Steady-State Absorption Spectra. The electronic absorption spectrum of porphyrins and its derivatives has been extensively studied and is well characterized in the literature.[26] The spectrum of free base porphyrins, like TMPyP (Figure 1), features an intense band around 420 nm known as the Soret band, which corresponds to the S_2 transition. Toward the long-wavelength region, four satellite bands are found, which were assigned to a pair of vibronic progressions corresponding to the S_1 transition.

The changes in the absorption spectra of TMPyP with the addition of PAMAM dendrimers were followed maintaining the concentration of porphyrin at 5 μM, below its self-aggregation threshold,[12c] and increasing the concentration of dendrimer from molar ratios (D/P ≡ [PAMAM]/[TMPyP]) of 0.05 up to 20.

The Soret band displays a red shift of about 5−6 nm with increasing D/P (Figure 1, inset). The absorption spectra for generation 4.5 are omitted in Figure 1, since similar effects were observed, although they are displaced to lower D/P ratios in comparison to generation 2.5. The absence of clear isosbestic points for both generations studied suggests that the association of TMPyP with PAMAMs is not a simple equilibrium between free and complexed species. However, this is not a straightforward conclusion, since it is difficult to obtain exact reproducibility in the values measured for absorbance. This is also valid for other quantities monitored in these systems, in particular for the D/P ratios near the inflection point in the plots versus dendrimer concentration (e.g., absorption maxima, relative quantum yield, fluorescence lifetimes, anisotropy, and pH). For this reason, additional attention was devoted to D/P ratios of 1 and 10 in the systems with generation 2.5, to give examples of a system near the inflection point and another in the plateau region at high dendrimer concentrations, respectively. In the case of steady-state emission, several measurements with different samples were performed in these systems, to estimate the uncertainty interval associated with the quenching effect observed, as is presented in the next subsection.

In a single experiment, the concentrations of both TMPyP and PAMAM were varied from 25 to 2.5 μM, keeping the D/P ratio at 1, and changes in the absorption spectrum were followed up. The dilution induces dissociation of the porphyrin−dendrimer complex to give free porphyrin and dendrimer species. The absorbance at 400 nm is depicted in Figure 2, and although it resembles a plot of Beer's law for the porphyrin−dendrimer complex, it is not, since dissociation is also occurring, as is noticeable from the shift in the Soret maximum depicted

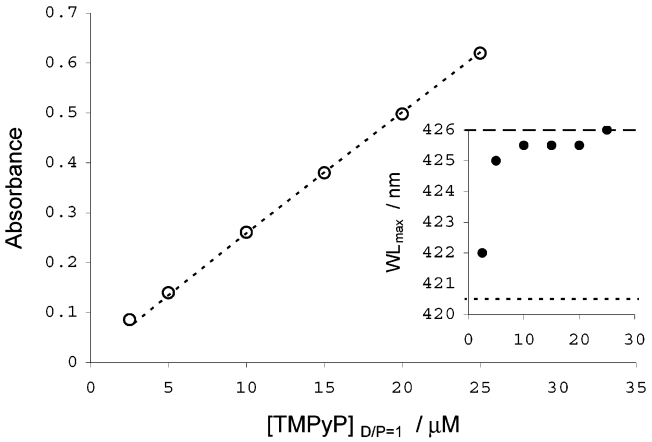

Figure 2. Variation of TMPyP absorbance at 400 nm in the system with generation 2.5 PAMAMs and a constant D/P ratio of 1 (the dotted line was fitted with a 1:1 complexation model). The inset shows the shifts of the Soret band maximum for the same concentrations (the dotted line indicates the Soret peak position for free TMPyP, and the dashed line is the same for the complex with generation 2.5, D/P = 10).

in the inset of this figure. A simple 1:1 association equilibrium model was used to fit the experimental points (dotted line in Figure 2). In this model, the absorptivity of complexed TMPyP at 400 nm was estimated from the absorption spectrum at D/P = 10, assuming nearly complete association in this case. The value obtained for the association constant was $5.75 \times 10^7\ M^{-1}$, which shows the high binding affinity of the porphyrin and dendrimer species.

Steady-State Fluorescence Quenching. The emission spectrum of TMPyP changes significantly with solvent polarity. The vibrational structure of TMPyP's emission spectrum in aqueous solution is severely masked due to band broadening, and the *Q*(0,0) emission band appears as a shoulder relative to the more intense *Q*(0,1) band. An explanation proposed in the literature for this behavior invokes mixing of the S_1 state with a nearby charge-transfer (CT) state, mediated through the librational motion of the *meso N*-methylpyridinium groups.[12c] In less polar solvents, like methanol, this CT state would be destabilized, precluding its electronic coupling with the S_1 state, and the emission spectrum would preserve its vibronic resolution.

A strong fluorescence quenching effect was observed for TMPyP in the presence of PAMAM dendrimers for both generations studied (Figure 3). Additionally, an increase in the spectrum's vibronic resolution was also observed. Accordingly, this effect could be ascribed either to a decrease in the polarity of TMPyP's surrounding environment in the associated form or to restraints in the vibrational motion of TMPyP's *N*-methylpyridinium groups upon binding to the dendrimer's terminal groups.

The Stern−Volmer representation of the fluorescence quenching results clearly reveals a nonlinear trend for both generations. These are represented in Figure 4 using a semilog plot to offer a better perception of the low D/P region (it should be noticed that the D/P ratio is directly proportional to the quencher concentration, as in the classical Stern−Volmer plot, since TMPyP is present at constant concentration). In contrast, the plateau region obtained in the limit of high D/P ratios is better seen in a linear-scale representation (not shown). In this case, the excess of dendrimer concentration should lead to complete association of TMPyP. From the limiting value of ϕ^0/ϕ, it is possible to estimate that the porphyrin−dendrimer complex is 15 and 20% less emissive than free TMPyP for generations 2.5 and 4.5, respectively.

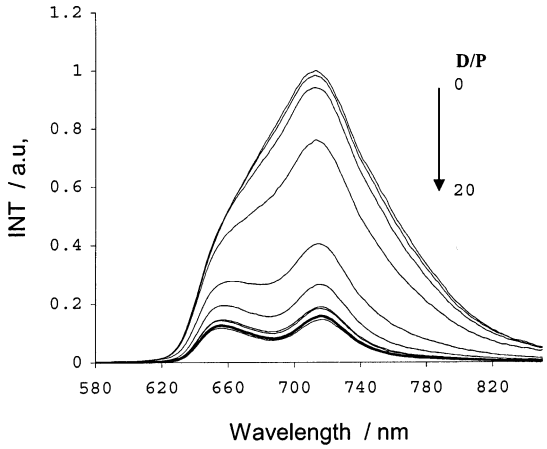

Figure 3. Fluorescence spectra of aqueous TMPyP in the systems with PAMAM dendrimers of generation 2.5 and D/P ratios of 0, 0.2, 0.4, 0.5, 0.8, 1, 2, 3, 5, 10, and 20 (excitation at 400 nm, solid lines correspond to D/P ratios of 0, 1, and 10, from top to bottom, respectively).

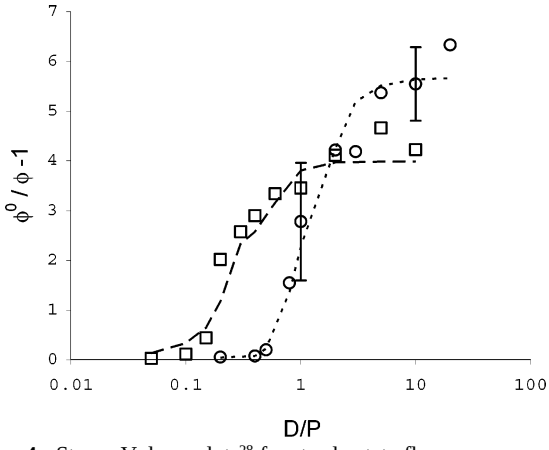

Figure 4. Stern−Volmer plots[28] for steady-state fluorescence quenching of TMPyP induced by PAMAM dendrimers of generation 2.5 (open circles) and 4.5 (open squares). The dotted and dashed lines were modeled with the Fuoss equation for generations 2.5 and 4.5, respectively (see the Discussion for further details).

The reproducibility issue raised in the last subsection, regarding the D/P ratios near the inflection point, is recovered in Figure 4, which presents the error bars (only) for D/P ratios of 1 and 10 in the system with generation 2.5. These were estimated from the standard deviation of seven and four measurements (with different samples) for D/P = 1 and 10, respectively, affected by the corresponding *t*-student parameter with 95% confidence. It is clear that the experimental uncertainty is greater in the vicinity of the inflection point, which is a very steep part of the Stern−Volmer curve. Therefore, it is a difficult task to retrieve accurate values from fitting the experimental results with a physical model. Instead, it is preferable to make some assumptions, based on experimental observations, regarding the process of fluorescence quenching and then to use a model to reproduce the behavior observed. This was attempted in the framework of the Fuoss equation[27] for the ion-pair stability constant, K_A, which depends crucially on the charge, Z_i, and radius, R_i, assumed for the species involved (i = A or B and $R = R_A + R_B$).

$$K_A = \frac{4\pi N_A R^3}{3} \exp\left[-\frac{U(R,\mu)}{k_B T}\right] \qquad (1)$$

This dependence can be made explicit using, for instance, the

Debye−Hückel expression for the electrostatic potential

$$U(r,\mu) = \frac{Z_A Z_B e^2}{4\pi\epsilon\epsilon_0 r}\left(\frac{\epsilon^{\beta\sigma_A\sqrt{\mu}}}{1+\beta\sigma_A\sqrt{\mu}} + \frac{\epsilon^{\beta\sigma_B\sqrt{\mu}}}{1+\beta\sigma_B\sqrt{\mu}}\right)\exp(-\beta r\sqrt{\mu}) \quad (2)$$

where μ is the ionic strength, σ_i is the radius of species i plus that of the dominant counterion, and β is given by

$$\beta = \frac{e^2}{4\pi\epsilon\epsilon_0 k_B T} \quad (3)$$

The results are shown in Figure 4, depicted as dotted and dashed lines for generations 2.5 and 4.5, respectively. Since the assumptions made in this modeling procedure are rather intricate, these are further developed in the Discussion section.

Some insight concerning the quenching effect was gained from steady-state absorption and emission spectra of TMPyP in an aqueous solution of simple organic compounds with the same functional groups present in PAMAM dendrimers. In this sense, triethylamine, *N*-ethylacetamide, and propionic acid were employed to mimic, respectively, the core/branching units, the repeating units, and the terminal groups of half-generation PAMAM dendrimers. Similar concentrations of the functional groups within the dendrimers' volume (estimated from the hydrodynamic radius reported for these molecules[29,30]) were employed. The more intuitive results were obtained for the interaction of TMPyP with triethylamine, in which case a larger red shift of the Soret band was observed. Furthermore, it is only for triethylamine that fluorescence quenching is observed, although an increase in the vibrational resolution of the emission spectrum occurs in all cases. It is reasonable to assume that the tertiary amines, which constitute the branching points in the PAMAM's structure, are responsible for the quenching of TMPyP fluorescence upon dendrimer association. Tertiary amines are known for their electron-donating character (low ionization potential) in photoinduced charge-transfer reactions, and some simple thermodynamic considerations show that such a mechanism is not excluded between TMPyP and triethylamine. Taking the oxidation potential of triethylamine, $E°(NEt_3^{\bullet+}/NEt_3) = 1.211$ V,[31] along with the reduction potential of TMPyP, $E°(TMPyP/TMPyP^{\bullet-}) = -0.23$ V,[12a] and its respective 0−0 excitation energy, $\Delta E_{0-0} = 1.83$ eV, the free energy change for electron transfer to the singlet excited state of TMPyP, $\Delta G°$, can be assessed from[32] $\Delta G° = E°(NEt_3^{\bullet+}/NEt_3) - E°(TMPyP/TMPyP^{\bullet-}) - \Delta E_{0-0}$ to be −0.389 eV (−37.5 kJ·mol^{-1}), which shows that this process is thermodynamically favorable. The same quenching mechanism was assumed for systems with PAMAM dendrimers.

Time-Resolved Fluorescence. Fluorescence decays of TMPyP alone in water are biexponential with a major component of about 5 ns and a second one with a variable weight and a lifetime around 1 ns (Table 1). The interpretation of these lifetime components has been discussed in the literature, mostly in parallel with the aggregation behavior of this porphyrin. Kemnitz et al. initially attributed the long- and short-lifetime components to the dimer and monomer of TMPyP, respectively, and performed temperature-dependent experiments to assess the thermodynamic properties of monomer−dimer equilibrium.[14b] However, the lack of definite evidence to corroborate the self-aggregation of this porphyrin for concentrations lower than 10^{-3} M prompted the proposal of alternative explanations. In this sense, Vergeldt et al. attributed the short lifetime to the adsorption of TMPyP at solid surfaces and proposed that the dispersion of values reported for the weight of this component results from differences in the experimental setup geometry used for the determination of fluorescence lifetimes.[12c] Recently, other authors measured the fluorescence decay of TMPyP in front-face geometry and also reported two lifetimes: one long component with a similar value to that previously known and a short one with a lifetime of 300 ps.[15] These authors then argued that this latter component corresponds to TMPyP adsorbed at the cuvette walls and attribute the 1−2 ns component to the aggregate in solution, although the absence of this component in the front-face measurements was not explained.

TABLE 1: Lifetime Values Fitted to the Fluorescence Decays of TMPyP in the Systems with Generation 2.5 PAMAMs with a Multiexponential Expression (Excitation at 400 nm and Emission in the Range 600−800 nm)

D/P	τ_1/ns	τ_2/ns	τ_3/ns	χ^2
0	5.012 (96.8%)	1.515 (3.2%)		1.180
0.2	5.205 (90.4%)	2.578 (9.6%)		1.133
0.4	5.145 (94.4%)	1.655 (5.6%)		1.186
0.5	5.524 (67.4%)	3.369 (29.5%)	0.646 (3.2%)	1.075
0.8	4.978 (69.7%)	1.762 (25.3%)	0.419 (5.0%)	1.127
1	4.540 (55.0%)	1.618 (37.3%)	0.396 (7.7%)	1.104
2	4.004 (37.3%)	1.505 (50.9%)	0.384 (11.8%)	1.033
3	3.731 (35.2%)	1.514 (50.1%)	0.402 (14.7%)	1.137
5	3.384 (35.2%)	1.337 (52.2%)	0.345 (12.5%)	1.124
10	3.270 (34.9%)	1.285 (51.6%)	0.349 (13.5%)	1.139
20	3.102 (32.3%)	1.221 (53.7%)	0.328 (14.0%)	1.070

TABLE 2: Lifetime Values Fitted to the Fluorescence Decays of TMPyP in the Systems with Generation 4.5 PAMAMs with a Multiexponential Expression (Excitation at 400 nm and Emission in the Range 600−800 nm)

D/P	τ_1/ns	τ_2/ns	τ_3/ns	χ^2
0.05	5.029 (96.3%)	1.581 (3.7%)		1.043
0.1	5.035 (94.9%)	1.457 (5.1%)		1.114
0.15	4.980 (86.3%)	1.710 (12.3%)	0.221 (1.5%)	1.086
0.2	4.227 (53.5%)	1.475 (38.0%)	0.282 (8.4%)	1.058
0.3	3.795 (53.9%)	1.304 (39.0%)	0.251 (7.1%)	1.002
0.4	3.813 (47.5%)	1.472 (41.2%)	0.408 (11.3%)	1.092
0.6	3.519 (40.4%)	1.242 (47.8%)	0.305 (11.8%)	1.073
1	3.333 (44.1%)	1.168 (48.3%)	0.279 (7.7%)	1.101
2	3.484 (36.6%)	1.443 (48.6%)	0.428 (14.8%)	1.104
5	3.022 (46.1%)	1.087 (46.1%)	0.236 (7.8%)	1.143
10	3.527 (37.4%)	1.398 (51.2%)	0.345 (11.4%)	1.080

In the presence of PAMAM dendrimers, the fluorescence decays of TMPyP become more complex and at least three exponential components are required to obtain a proper fit (see Tables 1 and 2). The lifetime of the long component decreases from about 5 to 3 ns, while the second component varies between 1.8 and 1.2 ns (with some higher values off-trend). The short lifetime has values around 200−650 ps. Similar to the steady-state measurements, the major changes in the fluorescence decays occur over a small D/P range (Figure 5), and for high dendrimer concentrations, only little differences are observed. The Stern−Volmer plot for the integrated area of the decay curves (closed symbols in Figure 6) also reveals this feature. However, the total decay area seems to be overestimated and the quenching extent is apparently less, when compared to steady-state results (open symbols in Figure 6). This suggests that a static effect is taking place and that some short decay components are missed within the temporal resolution of these measurements.

Fluorescence Anisotropy. Steady-state fluorescence anisotropy increases with dendrimer concentration following a similar trend to the emission intensity (Figure 7). Even though the uncertainty of these measures is sometimes large, the steady-state anisotropy of TMPyP is clearly higher in the presence of PAMAM dendrimers, when compared to the free species in

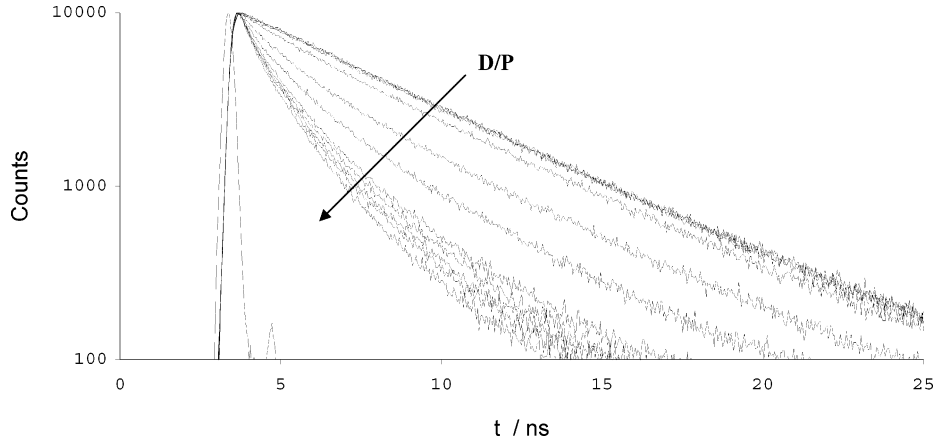

Figure 5. Fluorescence decays of TMPyP in the systems with PAMAM dendrimers of generation 2.5 and D/P ratios of 0, 0.2, 0.4, 0.5, 0.8, 1, 2, 3, 5, 10, and 20 (excitation at 400 nm and emission at 600−800 nm).

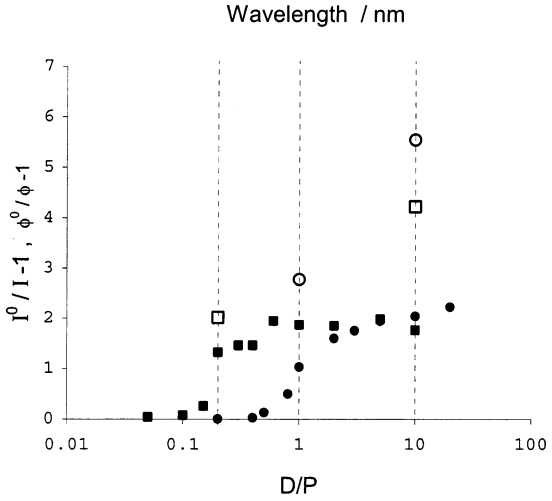

Figure 6. Stern−Volmer plot of the integrated area of fluorescence decays ($I = \int I(t)\, dt$) for TMPyP in the systems with PAMAM dendrimers of generation 2.5 (closed circles) and 4.5 (closed squares). The open symbols have the same meaning as those in Figure 4 and represent the equivalent values for steady-state results at D/P ratios chosen for comparison.

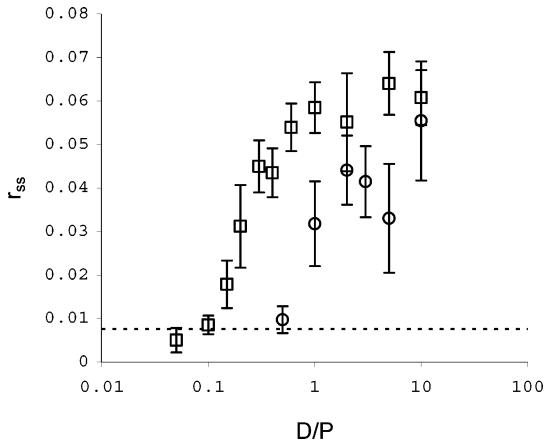

Figure 7. Steady-state fluorescence anisotropy of TMPyP in aqueous solution with PAMAM dendrimers of generation 2.5 (open circles) and 4.5 (open squares). Excitation was selected at 515 nm and emission was collected in the range 700−720 nm.

aqueous solution. The limiting anisotropy, r_0, value of this porphyrin for excitation at 515 nm and emission in the interval 700−720 nm was estimated from the Perrin formula[33] using its fluorescence and depolarization lifetimes in aqueous solution (without dendrimer) and gave a value of 0.144 ± 0.062. This r_0 value is comparable to values reported in the literature for excitation in the second vibronic of the *Q* bands.[34] However, it differs completely from the theoretical value that would be expected assuming that the absorption and emission transition dipoles are strictly perpendicular. Probably there is some overlap of vibronics from Q_x and Q_y band progressions at the excitation wavelength. The Perrin formula was again employed to estimate the steady-state anisotropy, r_{SS}, at high dendrimer concentrations, assuming that fluorescence depolarization comes from rotation of the porphyrin−dendrimer complex as a single entity (tight-binding complex). For this purpose, the Stokes−Debye−Einstein equation[33] was used to estimate the rotational lifetime of PAMAM dendrimers of generations 2.5 and 4.5 using the hydrodynamic radius estimated from the literature.[29,30] The fluorescence lifetime was taken as the square-average from the three exponential components fitted to fluorescence decays at D/P = 10. This afforded r_{SS} values of 0.116 ± 0.050 and 0.136 ± 0.058 for generations 2.5 and 4.5, respectively. These values are somewhat higher than the experimental ones (at D/P = 10), even considering the overlap of the uncertainty intervals for the estimated and experimental values. Probably there is some librational or translational freedom for the porphyin in the complex that accounts for the additional depolarization observed.[35,36] Some preliminary studies of time-resolved fluorescence anisotropy also support this hypothesis. The anisotropy decays at high dendrimer concentrations are single exponential with depolarization lifetimes of 1.69 and 2.50 ns for generations 2.5 and 4.5, respectively. These values are significantly lower than those estimated from the Stokes−Debye−Einstein equation, which gave values of 7.72 and 32.3 ns for the same generations. Therefore, the tight-binding model for the porphyrin−dendrimer complex is not appropriate and some motional freedom has to be allowed in order to explain the fluorescence anisotropy results.

Ionic Strength Effect. To further assess the electrostatic nature of TMPyP association to half-generation PAMAM dendrimers in aqueous solution, the ionic strength for the systems with D/P = 10 was varied by adding sodium chloride. The effects were followed up using the same techniques as before. In generation 2.5, the changes observed are in accordance with a gradual decrease of porphyrin−dendrimer interaction with increasing ionic strength. The loss of red shift in the Soret band of TMPyP occurs with a concomitant decrease of fluorescence quenching (Figure 8) and also steady-state anisotropy. However, in generation 4.5, these trends are only observed at higher salt concentrations and, in contrast, there is even an increase in fluorescence quenching at low salt concentrations. On the other hand, an isosbestic point is observed in the Soret region for

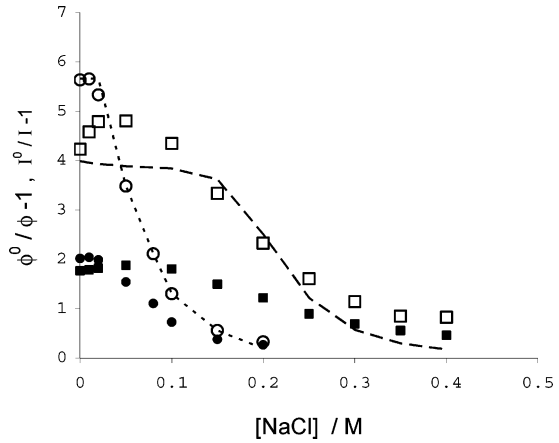

Figure 8. Effect of ionic strength in the steady-state (open symbols) and time-resolved (closed symbols) emission of TMPyP in the systems with PAMAM dendrimers of generation 2.5 (circles) and 4.5 (squares) for a D/P ratio of 10. The dotted and dashed lines are attempts to model the results with the Fuoss equation for generations 2.5 and 4.5, respectively (see the Discussion for further details).

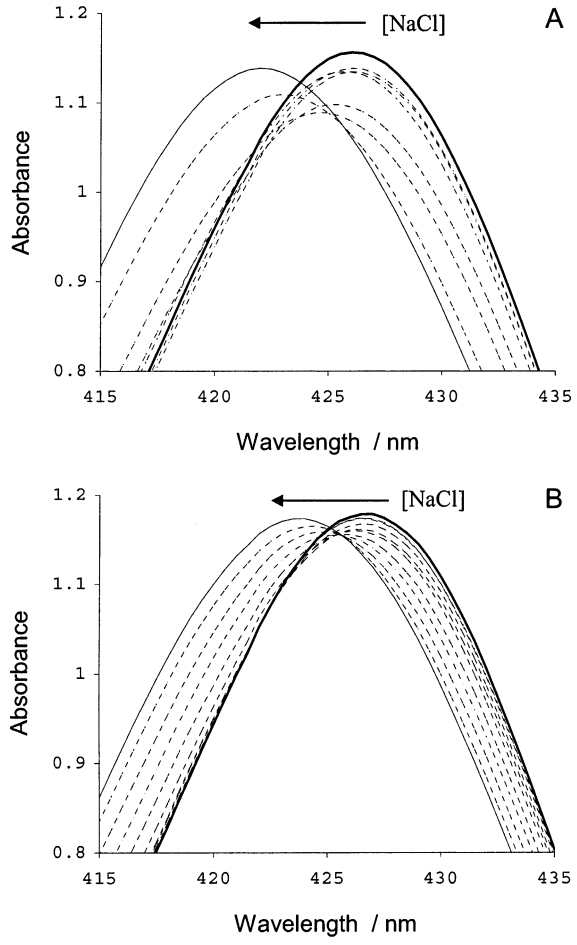

Figure 9. Effect of ionic strength in the absorption spectrum of TMPyP (Soret band) in the systems with PAMAM dendrimers of generation 2.5 (A) and 4.5 (B) at a D/P ratio of 10. The salt concentrations are the same as those in Figure 8 (solid lines are for the systems without added salt).

generation 4.5 but not for generation 2.5 (Figure 9). If the decrease of porphyrin−dendrimer association, observed for both generations, with increasing salt concentration is qualitatively explained in the context of the Fuoss model, the same is not valid for the absence of isosbestic points for generation 2.5 and the increase of the quenching effect at low salt concentrations for generation 4.5. These difficulties are obvious when the Fuoss equation is used to model the ionic strength effect in the system with generation 4.5 (dashed line in Figure 4). Some other effects not contained in the Fuoss classical model, either of electrostatic nature or not, must affect porphyrin−dendrimer association. These are discussed next.

4. Discussion

Steady-State Fluorescence Quenching. In this section, the results presented before are discussed in the context of some simple electrostatic models. This is the case of the Fuoss equation for the stability constant of ion pairs, which treats these species as charged spheres embedded in a dielectric continuum. It is assumed that TMPyP associates with half-generation PAMAMs, forming an ion-pair complex with an average fluorescence quantum yield lower than that of free TMPyP due to the possibility of a photoinduced electron-transfer (PET) process with the tertiary amine groups in the dendrimer. This assumption explains the plateau observed in the Stern−Volmer plots (Figures 4 and 6) for D/P ratios above one, even though the absolute concentration of dendrimer is not very high. Applying such a model to the systems studied is not straightforward, in particular, concerning the choice of parameters for PAMAM dendrimers. These macromolecules behave as polyfunctional bases due to the carboxylate terminal groups and to the tertiary amines in the branching points. Thus, the actual charge of the macroion is conditioned by the pH of the medium. In addition, the bulky number of charged terminal groups, in higher generations, induces a large surface potential and counterion condensation begins to regulate the dendrimers' effective charge. These effects are addressed in appendixes A and B.

Reasonable estimates for the dendrimers' effective charge are only possible if the protonation state is known, to evaluate charge renormalization from counterion condensation. For this reason, the Fuoss equation was applied here for illustration purposes only, with the dendrimer's effective charge being adjusted to model the behavior of the Stern−Volmer curves obtained (see appendix C for details). In the case of generation 2.5 (open circles in Figure 4), the results were modeled considering only 1:1 porphyrin−dendrimer association. A reasonable description of the Stern−Volmer curve was obtained by assuming a fluorescence quantum yield for the porphyrin−dendrimer complex that is 15% that of free TMPyP and by gradually changing the dendrimer's charge from −6 to −10, as its concentration increases. Such charge variation would have to be justified with the increase in pH (see Figure 12 in appendix A) and ionic strength with dendrimer concentration.

In contrast, in modeling the Stern−Volmer plot of generation 4.5 (open squares in Figure 4), porphyrin−dendrimer complexes with stoichiometries of up to 4:1 had to be allowed, to fairly describe the shape of the curve. This is not unrealistic considering the size (31.9 Å) and the estimated effective charge (minimum of −27.9) of this generation. The association equilibrium constants for several complexes were determined with the Fuoss equation using the same parameters, except for the dendrimer charge which increases +4 with each associated porphyrin. The mass balance for each dendrimer concentration was solved numerically through an iterative procedure and the fraction, f_i, of light absorbed by each complex was determined from

$$f_i = \frac{(1 - 10^{-\epsilon_i l[\mathrm{P}_i,\mathrm{D}]})}{(1 - 10^{-\epsilon_0 l[\mathrm{P}]}) + \sum_{j=1}^{n}(1 - 10^{-\epsilon_j l[\mathrm{P}_j,\mathrm{D}]})} \qquad (4)$$

where ϵ_i is the absorption coefficient of TMPyP for $i = 0$ and of $\{P_i,D\}$ for $i \neq 0$ at the excitation wavelength (l is the optical path length, and n is 4). These values were taken from the absorption spectrum of TMPyP in aqueous solution: without dendrimer for $i = 0$ and with a large excess concentration of dendrimer for $i \neq 0$. The average relative quantum yield is given by the following expression

$$\frac{\phi^0}{\phi} = \left[(1 - \sum_{i=1}^{n} f_i) + \sum_{i=1}^{n} f_i \frac{\phi_i}{\phi^0}\right]^{-1} \quad (5)$$

where ϕ_i is the fluorescence quantum yield of TMPyP for $i = 0$ and of $\{P_i,D\}$ for $i \neq 0$. The latter were adjusted by trial and error to fit the Stern−Volmer curve, and the values achieved increase from 20 to 30% relative to ϕ^0, as the number of associated porphyrins increases from 1 to 4. Such variation is tentatively explained considering a perturbation of the porphyrin−dendrimer complex with the increasing number of binded porphyrins that would lead to a decrease of the quenching efficiency by the dendrimer. The values used for the dendrimer's effective charge vary from −37.8 to −27 and were estimated assuming a degree of protonation corresponding to an average pK_a of 9 for the outer layer tertiary amines and correcting for the counterion condensation with the Poisson−Boltzmann (PB) model. No real significance should be attributed to this variation, since for such a high charge density the model (expression 5 and previous) is not sensitive enough to discern between these values of charge.

This approach fails unequivocally to explain the trends observed with ionic strength. In the case of generation 2.5, the charge of the dendrimer would have to increase up to −32 (its maximum value) to describe the residual quenching effect at high salt concentrations (dotted line in Figure 8). On the other hand, for generation 4.5, it is not possible to explain the initial increase in the fluorescence quenching at low salt concentrations, even assuming the higher possible charge of −128 for this generation (dashed line in Figure 8). This reveals that aspects not taken into consideration in the framework of simple electrostatics must be important in these systems, for instance, the role of dispersion forces (van der Waals interactions) or specific interactions (hydrogen bonding) in porphyrin−dendrimer association. The approximation of these molecules to charged hard spheres is also questionable, in particular for PAMAM dendrimers, which have flexible structures and in solution assume an ellipsoidal oblate shape. It is possible that a conformational response of the porphyrin−dendrimer complex to the increase of ionic strength leads to higher quenching efficiencies in generation 4.5 at low salt concentrations. Some effort has been reported in the literature to experimentally assess the influence of solvent quality or pH and ionic strength in aqueous medium on the dendrimer's structure (and so its radius) in solution.[29,37] This could be relevant for the models applied here, since these depend on the radius of the species involved.

Fluorescence Decays at High D/P Ratios. As it was previously mentioned, a static effect was detected by comparison of steady-state and time-resolved fluorescence results. This implies that ultrafast components, occurring in these systems, are not accessible within the temporal resolution of tens of picoseconds. Such high quenching rates are possible for PET processes. Furthermore, the multiexponential decays at high D/P ratios could be attributed to a distribution of rate constants for PET within the porphyrin−dendrimer complex. Such a distribution could arise simply from the availability of multiple tertiary amines (donors) in the dendrimer structure with different relative distances to the porphyrin (acceptor). In the framework of semiclassical Marcus theory, the ET rate depends on the distance essentially through the electronic coupling Hamiltonian element and the reorganization energy parameter. The distance dependence of the former is usually expressed as a damped exponential function, and a distribution of damping factors could also be invoked in the dendrimer.[38] Alternatively, it could be argued that the flexible structure of PAMAMs offers a conformational manifold for the porphyrin−dendrimer complex with different PET efficiencies for each subset and that the rate distribution observed reflects the interconversion dynamics between these.[39] These features were neither explicitly included in the modeling procedure used for the steady state nor explicitly included for the time-resolved fluorescence. In the former case, it was considered that the porphyrin−dendrimer complex has an average fluorescence quantum yield, which was estimated to be 15−20% relative to free TMPyP. The fluorescence decays for the porphyrin−dendrimer complex were fitted with a dispersed kinetics model that considers a Gaussian distribution of the logarithm of quenching rates.[40]

$$I(t) = A \exp\left(-\frac{t}{\tau_0}\right) \times \frac{1}{\sqrt{\pi}} \int_{-\infty}^{+\infty} \exp(-x^2) \times \exp[-k^i_{ET,0} \exp(\gamma x) \times t]\, dx \quad (6)$$

where τ_0 is the intrinsic decay lifetime of TMPyP in the dendrimer "environment", x is a random variable associated with the distribution of quenching rates, and γ is a parameter related to its variance, while $k^i_{ET,0}$ is the value of the quenching rate constant in the distribution peak. The actual interpretation of this distribution in the systems studied is not straightforward for the reasons given above and also because of the experimental limitation to detect ultrafast components. However, there is some economy in the number of parameters required to describe the fluorescence decays at high D/P ratios, by comparison with a multiexponential analysis. Thus, only the values fitted for the fluorescence decay of TMPyP in the system with generation 2.5 and D/P = 10 are presented here, since these were used in the model proposed in the next subsection for intermediate D/P ratios. The retrieved values were the following: $\tau_0 = 6.27$ ns, $k^i_{ET,0} = 1.03 \times 10^9$ s^{-1}, and $\gamma = 1.55$, with a χ^2 value of 1.133 and a Durbin−Watson parameter of 1.825 for the fit. There will only be some brief remarks about these values. The slightly higher lifetime of complexed TMPyP is in agreement with a less polar environment in the dendrimer (e.g., the major lifetime of TMPyP fluorescence decay in methanol is about 10 ns).[12c] The $k^i_{ET,0}$ value is within experimental resolution and is comparable to the average value estimated from multiexponential analysis. Finally, the γ value is similar to values reported in the literature for other systems.[41]

Fluorescence Decays at Intermediate D/P Ratios. In this situation, the porphyrin−dendrimer complex exists in equilibrium with a population of free TMPyP. It then becomes necessary to consider additional processes to describe the excited-state behavior of TMPyP, for instance, interconversion between free and complexed TMPyP or PET reaction at separations greater than the contact distance. A general proposition is given in Scheme 1. Some dark steps are included for completeness, for example, the back electron-transfer (bET) reaction of the solvent-separated radical pair and of the porphyrin−dendrimer radical complex (dotted arrows). These processes derive from excited-state deactivation and do not directly affect the fluorescence decay of TMPyP.

SCHEME 1

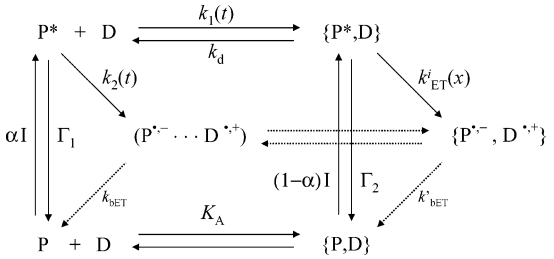

Time-dependent reaction rates were allowed for the porphyrin−dendrimer association step in the excited state, $k_1(t)$, and also for the PET process, $k_2(t)$, to include transient effects from electrostatically assisted diffusion over the short distances imposed by the nonrandom spatial distribution of reactants and also from the distance dependence of the ET reaction. Several authors have studied diffusion-controlled reactions between charged species, and approximate expressions for the time-dependent reaction rate, $k(t)$, have been proposed in the framework of the Debye−Smoluchowski−Collins−Kimball (DSCK) theory.[42−44] For instance, Flanery and co-workers arrived at one analytical solution of the time-dependent DSCK equation, which has the same functional form of $k(t)$ for noninteracting species. However, this model is only valid for $R \geq |Z_{\pm} \cdot l_B|$, where R is the collisional radius (sum of the reactants' radii), $Z_{\pm}$ is the reactant charge product, and l_B is the Bjerrum length ($l_B = e^2/\{4\pi\epsilon\epsilon_0 k_B T\}$). For the systems studied here, the R values are around 2.7 and 3.9 nm for generations 2.5 and 4.5, respectively,[45] while the calculated $|Z_{\pm} \cdot l_B|$ values are 90.3 and 361.4 nm for the same generations.[46] Moreover, analytical expressions known for time-dependent reaction rates were obtained with absorptive boundary conditions, which considers that reaction occurs only at a definite distance, R. On the other hand, if electron transfer is responsible for fluorescence quenching, then distance-dependent reaction rates, $k_{ET}(r)$, should be expected.

To formulate an appropriate description of the systems studied, the Sano−Tachiya equation for the pair survival probability, $w(\mathbf{r},t)$, was used to model the mutual diffusion of the reactants.[47,48]

$$\frac{\partial w(\boldsymbol{r},t)}{\partial t} = D\left[\nabla^2 w(\boldsymbol{r},t) - \frac{1}{k_B T}\nabla U \cdot \nabla w(\boldsymbol{r},t)\right] \quad (7)$$

For the step with PET reaction, $k_2(t)$, a sink term, $-k_{ET}(\mathbf{r}) \cdot w(\mathbf{r},t)$, was added to the right-hand side (rhs) of expression 7. For spherically symmetric systems, this expression simplifies to

$$\frac{\partial w(r,t)}{\partial t} = D\left[\frac{\partial^2 w(r,t)}{\partial r^2} + \left(\frac{2}{r} - \frac{1}{k_B T}\frac{dU(r)}{dr}\right)\frac{\partial w(r,t)}{\partial r}\right] - k_{ET}(r)\, w(r,t) \quad (8)$$

where D is the mutual diffusion coefficient (sum of the diffusion coefficients of the reactants) and $U(r)$ is the interaction potential for the reacting species. Coulomb potential was assumed here. For the electron-transfer rate, the following expression was used: $k_{ET}(r) = \nu_0 \exp[-\beta(r - R)]$, where ν_0 stands for the reaction rate at the collisional distance R and β is the "damping" factor. This approach is equivalent to considering the semiclassical expression of Marcus ET theory with the exponential distance-dependent electronic coupling term, H_{AB}^2, and neglecting the distance dependence of the reorganization energy, λ.[49]

In the case of $k_1(t)$, the initial and boundary conditions applied were the following:

$$w(r,0) = 1 \quad (9)$$

$$4\pi R^2 D \times \left[\frac{\partial w(r,t)}{\partial r}\right]_{r=R} = p w(R,t) \quad (10)$$

$$w(\infty,t) = 1 \quad (11)$$

with a high numerical value for p to have absorptive boundary conditions. In contrast, for $k_2(t)$, in which case ET reaction occurs before association, reflective boundary conditions were used ($p = 0$). The numerical solution of eq 8 provides the survival probability functions of the reactant pair, $w_i(r,t)$ ($i = 1$, without the sink term and $p = \infty$ or $i = 2$, with the sink term and $p = 0$), that are used in expression 12 to calculate the respective δ-response reaction rates, $k_{i\delta}(t)$, from which the $k_i(t)$ rates can be derived.

$$k_{i\delta}(t) = \frac{d}{dt}\{C_B \times \int_R^{\infty}[1 - w_i(r,t)] \exp(-U(r)/k_B T) r^2\, dr\}, \quad i = 1,2 \quad (12)$$

Here, C_B is the quencher concentration and the other symbols have the usual meaning.

The systems modeled were those with generation 2.5 and D/P ratios of 0.8, 1, and 2 (i.e., near the inflection point of the Stern−Volmer curve). The diffusion coefficients of the reacting species were estimated from the Stokes−Einstein equation, $D_{A/B} = k_B T/(4\pi\eta R_{A/B})$, and this afforded a value of 6.53×10^{-10} m^2 s^{-1} for the mutual diffusion coefficient, $D = D_A + D_B$, assuming values of 7 and 19.8 Å for the porphyrin and dendrimer radii, respectively. The collisional radius, R, is therefore 26.8 Å. The structural charge of TMPyP, +4, was assumed for the electrostatic potential, $U(r)$. On the other hand, the dendrimer's charge was obtained from the steady-state results using the Fuoss equation, as previously explained, and this gave values around −6. The electric permittivity of the medium was fixed at the value for water at room temperature ($\epsilon = 79.5$). Concerning the reaction rate at the collisional distance, ν_0, a value of 1×10^9 s^{-1} was employed to approximately match the value of $k^i_{ET,0}$ fitted from the fluorescence decay of the porphyrin−dendrimer complex. The damping factor was assumed to be 1 Å^{-1}, which is a typical value for several electron-transfer reactions.[49]

Scheme 1 was solved for the excited-state free porphyrin, P*, and its complexed form, {P*,D}, using linear response formalism[50]

$$[P^*] = \alpha I \otimes f_1 + (1 - \alpha) I \otimes J \otimes (k_d f_2) \otimes f_1' + \alpha I \otimes J \otimes (k_{1\delta} f_1) \otimes (k_d f_2) \otimes f_1' \quad (13)$$

$$[\{P^*,D\}] = (1 - \alpha) I \otimes J \otimes f_2 + \alpha I \otimes J \otimes (k_{1\delta} f_1) \otimes f_2 \quad (14)$$

where $\otimes$ denotes the convolution integral operating on adjacent terms. Here, α is the fraction of photons absorbed by free porphyrin and I is the total number of moles of photons absorbed by unit time and volume. The f_1 and f_1' terms are the survival probabilities of P* directly excited by light absorption and of P* produced from the dissociation of {P*,D}, respectively. The f_2 term is the survival probabilities of {P*,D}

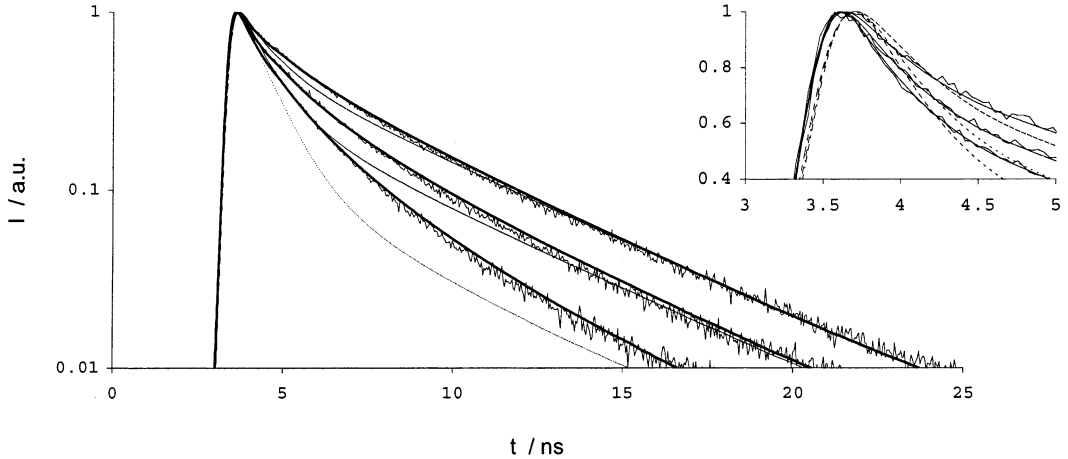

Figure 10. Decay curves estimated from numerical solution of Scheme 1 with $k_d = 0$ (solid lines) and $k_d = 10^{10}$ s^{-1} (dotted lines) overlaid with normalized fluorescence decays of TMPyP in the systems with generation 2.5 and D/P ratios of 0.8, 1, and 2 (thin gray lines) from top to bottom, respectively. The inset shows a magnification of the curve behavior at short times on a linear scale.

$$f_1 = \exp(-\Gamma_1 t)\exp\left(-\int_0^t k_{1\delta}(u)\,du\right)\exp\left(-\int_0^t k_{2\delta}(u)\,du\right) \quad (15)$$

$$f_1' = \exp(-\Gamma_1 t)\exp\left(-\int_0^t k_{1\delta}'(u)\,du\right)\times \exp\left(-\int_0^t k_{2\delta}(u)\,du\right) \quad (16)$$

$$f_2 = \exp(-\Gamma_2 t)\exp(-k_d t)\times\frac{1}{\sqrt{\pi}}\int_{-\infty}^{+\infty}\exp(-x^2)\times \exp[-k_{ET,0}^{i}\exp(\gamma x)\times t]\,dx \quad (17)$$

where Γ_1 and Γ_2 are the intrinsic decay rate constants of P* and {P*,D}. Expressions for the $k_{i\delta}(t)$ terms have already been given, and k_d is the dissociation rate constant of {P*,D}. The last term on the rhs of expression 17 is the survival probability toward ET reaction within {P*,D}, and it was introduced in the previous subsection.

The secondary production term, J, is given by

$$J = L^{-1}\left[\frac{1}{1 - L(k_{1\delta}'f_1')\times L(k_d f_2)}\right] \quad (18)$$

where L is the Laplace transform operator and L^{-1} its inverse. Finally, $k_{1\delta}'$ is obtained from $k_{1\delta}$ through the following expression

$$k_{1\delta}' = k_{1\delta} - \frac{d\ln k_{1\delta}}{dt} \quad (19)$$

Basically, it is a correction for the geminate pair recombination, in which case a pair of reactants at a contact distance exists superimposed with the general distribution of reactants (as considered for $k_{1\delta}$ alone, which is not necessarily a random distribution).

As previously mentioned, instead of fitting the fluorescence decays to such a complex model, it was preferred to make use of appropriate guesses for the respective parameters and then to compare the simulated curves with the experimental decays (for generation 2.5 and D/P = 0.8, 1, and 2). For this purpose, the I term in expressions 13 and 14 was replaced with the instrumental response function. The α fraction was evaluated from expression 4 with $i = 0$ and $n = 1$, by taking the species concentration from previous modeling of the steady-state Stern−Volmer curve with the Fuoss equation (this was initially done to check for agreement between both models). The convolution integrals and direct Laplace transform were numerically evaluated from the trapezoidal rule, and the inverse Laplace transform was obtained with the Gaver−Stehfest method. The kinetic traces of P* and {P*,D} obtained from expressions 13 and 14 were combined to give the global decay curve, which is experimentally observed.[51,52] Two situations were calculated: the case of irreversible association in the excited state, that is, $k_d = 0$, and the case of fast equilibrium between P* and {P*,D}, that is, $k_d = 10^{10}$ s^{-1}. These are depicted as full and dotted lines in Figure 10, respectively. It is clear that the irreversible case, with the parameter values used here, better reproduces the experimental behavior observed. This simplifies considerably the solution of Scheme 1, since it dismisses feedback and geminate pair recombination effects from excited-state equilibrium

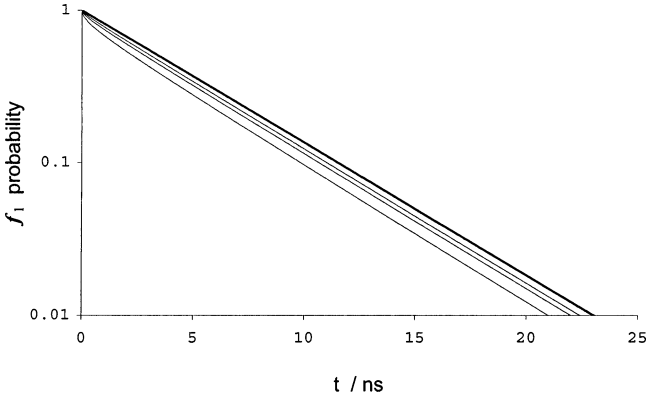

Figure 11. f_1 probabilities calculated from expression 15 for dendrimer concentrations equivalent to D/P ratios of 0 (full), 0.8 (dotted), 1 (dashed), and 2 (thin lines).

$$[P^*] = \alpha I \otimes f_1 \quad (20)$$

$$[\{P^*,D\}] = (1-\alpha)I \otimes f_2 + \alpha I \otimes (k_{1\delta}f_1)\otimes f_2 \quad (21)$$

Furthermore, it was found that transient diffusional effects are not expressive enough to influence the decay curve in the situations modeled. In Figure 11, the survival probabilities, f_1, are plotted against its first term, $\exp(-\Gamma_1 t)$, which is the intrinsic survival probability of P*. The lack of unusual short-time behavior in these curves suggests that the static effect observed is, indeed, related to ultrafast decay components in the porphyrin−dendrimer complex and it is not a transient diffusional effect, as sometimes occurs in the solutions of diffusional models. For the systems considered here, such effects appear

at higher dendrimer concentrations. However, in this situation, almost complete porphyrin−dendrimer association takes place and the fluorescence decay is dominated by the behavior of this population. In contrast, if diffusional quenching were important in these systems, then the model used for the steady-state results would have to be extended, to include this process. The most accurate procedure would be to integrate the solutions of a partially diffusion-controlled reaction model, like the Sano−Tachiya model, and to fit the steady-state Stern−Volmer curve.

A brief remark about the systems with generation 4.5 is due. The respective fluorescence decays were not modeled with the same procedure, since multiple porphyrin−dendrimer association stoichiometries seem possible for this generation and extending Scheme 1 would give a very complex picture to be supported by the experimental results. Furthermore, considering that the behavior of fluorescence decays in the systems with generation 2.5 is approximately determined by the population of complexed TMPyP and since association is even stronger in generation 4.5, it seemed that applying this analysis procedure to the latter system would fail to bring additional insight.

5. Final Comments

The interaction of cationic porphyrin TMPyP with carboxylate-terminated PAMAM dendrimers of generations 2.5 and 4.5 was studied in water by steady-state absorption and emission spectroscopy and time-resolved fluorescence. Changes in the absorption and emission spectra of TMPyP indicate a less polar environment upon association with PAMAM dendrimers. These changes are accompanied with strong fluorescence quenching of TMPyP emission. An electron-transfer reaction from the tertiary amines, within the dendrimer structure, to the singlet excited state of TMPyP was proposed for the quenching mechanism. From the plateau in the Stern−Volmer curves, at high dendrimer concentrations, an average quantum yield of 15−20% was estimated for the porphyrin−dendrimer complex relative to free aqueous TMPyP. However, the multiexponential fluorescence decays at high dendrimer concentrations suggest that a distribution of ET rates exists for the porphyrin−dendrimer complex. A reasonable hypothesis to explain such a distribution is to allow some conformational freedom for the porphyrin−dendrimer complex. The steady-state and time-resolved fluorescence anisotropy results support this picture.

A reasonable description of the Stern−Volmer curves was achieved using the Fuoss equation for ion-pair association equilibrium constants, although the same model fails to explain the ionic strength effect in the systems with generation 4.5, where multiple association stoichiometries are possible.

The fluorescence decays of the porphyrin−dendrimer complex were fitted with a dispersed kinetics model. On the other hand, at intermediate dendrimer concentrations, it was necessary to evaluate possible diffusional quenching processes. These were modeled with the Sano−Tachiya pair survival probability equation and the global kinetics scheme was solved numerically with convolution techniques. This analysis dismissed transient diffusional effects as a possible cause for the static effect detected from comparison of steady-state and time-resolved fluorescence results.

Acknowledgment. This work was mainly supported by CQE IV, project POCTI/QUI/35398/2000, and by the program Praxis XXI − FCT through the Ph.D. grant BD 21698/99 conceded to P.M.R.P. Prof. F. C. De Schryver is gratefully acknowledged for the opportunity of a short-term visit at the Laboratory for Molecular Dynamics and Spectroscopy, Department of Chemistry, Katholieke Universiteit Leuven, Belgium. This short-term visit was financially supported by The European Science Foundation, under the ULTRA Programme on Femtochemistry and Femtobiology. Partial support by Fundação Calouste Gulbenkian is also gratefully acknowledged. P.M.R.P, would like to express his gratitude to C. A. T. Laia and J. A. B. Ferreira for helpful discussions about this work.

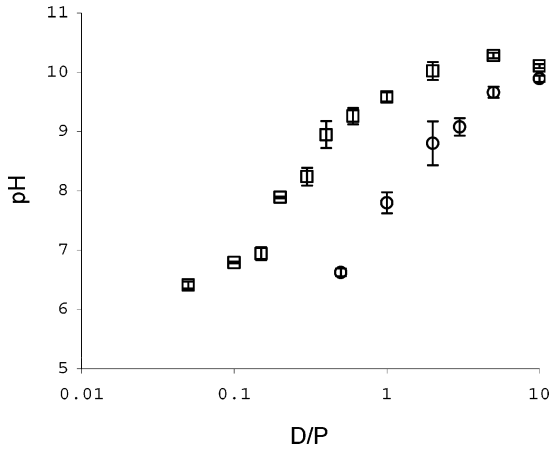

Figure 12. Values of pH measured for aqueous solutions of TMPyP and PAMAM dendrimers of generation 2.5 (open circles) and 4.5 (open squares).

Appendix A. Protonation Behavior of PAMAMs

The pH was measured for several D/P ratios to assess the protonation state of the PAMAM dendrimers (Figure 12). This requires knowledge of the equilibrium constants for each protonation site. The chemical structure of PAMAM dendrimers suggests that there are subsets of equivalent sites; however, the protonation sequence within them is not indifferent due to the energy cost for charging neighbor sites. A rigorous treatment of these effects was already developed and applied to full-generation PAMAMs.[53] It involves defining a site-binding model, by analogy to the classical Ising model, to include pair interactions between protonation sites (and higher order terms if necessary). Unfortunately, the cluster parameters necessary to estimate accurately the average protonation state of PAMAM dendrimers, using the pH values measured, are not available in the literature. It is safe to assume that the terminal carboxylate groups are deprotonated at these pH values, which accounts for 32 and 128 negative elementary charges in generations 2.5 and 4.5, respectively. Using as a reference a pK_a value of about 10 for the outer layer of tertiary amines in carboxylate-terminated poly(propyleneimine) (PPI) dendrimers,[54,55] it is possible that a relative decrease of the PAMAMs' effective charge occurs due to protonation of these amines.

Appendix B. Counterion Condensation in PAMAMs

To quantitatively evaluate the importance of counterion condensation for PAMAM dendrimers, the Poisson−Boltzmann (PB) cell model was employed (expression B.1), following a similar approach to that used for colloidal systems.[56]

$$\nabla^2\phi = \frac{1}{r^2}\frac{\mathrm{d}}{\mathrm{d}r}\left(r^2\frac{\mathrm{d}\phi}{\mathrm{d}r}\right) = 4\pi l_B N_A \sum_i c_i Z_i e^{Z_i\phi} \qquad \text{(B.1)}$$

Here, $\phi = -e\psi/k_BT$ is the reduced potential, N_A is the Avogadro number, Z_i is the charge of species i, and c_i is a constant which is related to its average concentration, C_i, through

$$C_i = c_i\langle e^{Z_i\phi}\rangle = \frac{c_i}{L^3/3}\int_a^L e^{Z_i\phi} r^2\,\mathrm{d}r \qquad \text{(B.2)}$$

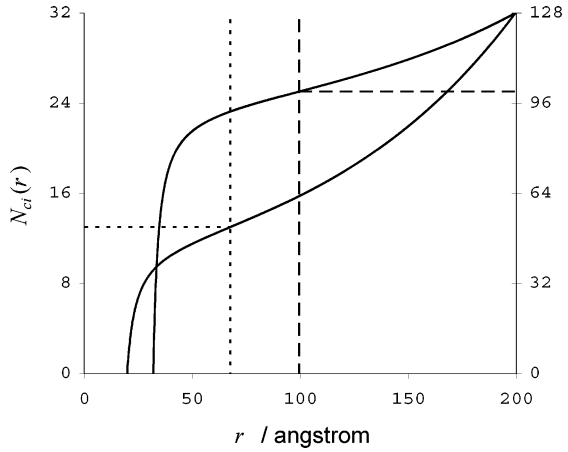

Figure 13. Counterion profiles estimated from the Poisson−Boltzmann model for PAMAM dendrimers of generation 2.5 (vertical axis to the left, dotted lines) and 4.5 (vertical axis to the right, dashed lines) at a concentration equivalent to D/P = 10. The vertical lines indicate the condensation threshold, *Y*, and the horizontal lines indicate the corresponding number of condensed counterions.

The integration is performed from the polyelectrolyte surface, *a*, to the edge of the spherical cell, *L*, which is calculated assuming that the counterionic shells do not overlap. Therefore, *L* is directly related to the polyelectrolyte concentration.

The boundary conditions used were trivial: $d\phi(L)/dr = 0$ and $\phi(L) = 0$. Numerical solutions of eq B.1 were obtained with the fourth-order Runge−Kutta method and accuracy was determined from comparison of $d\phi(a)/dr$ values obtained numerically with those calculated from $Z^{str}l_B/a^2$. Agreement is found typically below 0.10%. Other details are given elsewhere.[56b]

From the solutions of eq B.1, it is possible to obtain the ionic profiles through

$$N_i(r) = 4\pi\int_a^r c_i e^{Z_i\phi(s)} s^2\, ds \qquad \text{(B.3)}$$

The effective charge of the polyelectrolyte, Z^{eff}, is then calculated by assuming a threshold distance, *Y*, below which the electrostatic attraction of the counterions overcomes other interactions and these are considered to be condensed on the polyion.

$$Z^{eff} = Z^{str} + Z_{ci}N_{ci}(Y) \qquad \text{(B.4)}$$

The Bjerrum definition criteria, which uses the inflection point in the ionic profile, $d^2N_{ci}(Y)/dr^2 = 0$ to calculate the threshold distance, *Y*, was applied here. The structural charges, Z^{str}, of generation 2.5 and 4.5 PAMAMs were taken as −32 and −128, respectively, while the counterion charge, Z_{ci}, is +1 (sodium ion). This is equivalent to assuming that all carboxylate groups and tertiary amine groups are deprotonated and illustrates an extreme case of negative charge in the dendrimer. The results give a charge renormalization to values of −19.0 and −27.9 in generations 2.5 and 4.5, respectively (Figure 13). When protonation occurs the charge density (Z^{str}) of the dendrimer decreases and the PB model gives a smother effect of charge condensation.

Appendix C. Association Equilibrium for the Porphyrin−Dendrimer Complexes

The Stern−Volmer curves for steady-state emission were modeled assuming that the quenching effect is caused by the formation of porphyrin−dendrimer complexes with fluorescence quantum yields lower than free porphyrin and neglecting diffusional quenching processes (this is later confirmed to be approximately valid from the analysis of diffusional models). The successive equilibrium steps for the formation of multiple porphyrin−dendrimer complexes are

$$P + D \overset{K_{A1}}{\rightleftharpoons} \{P,D\} + P \overset{K_{A2}}{\rightleftharpoons} \ldots \overset{K_{An}}{\rightleftharpoons} \{P_n,D\}$$

where

$$K_{Ai} = \frac{[P_i,D]}{[P_{i-1},D][P]} \qquad \text{(C.1)}$$

The association constants, K_{Ai}, were estimated from the Fuoss equation (expressions 1 and 2) using the values indicated in the text for the model parameters. In particular, a constant value of $Z_A = +4$ was used for the porphyrin charge, while for the dendrimer it was assumed that the effective charge, Z^{eff}, increases by Z_A with each associated porphyrin, that is, $Z_B = Z^{eff} + i \times Z_A$ for the $\{P_i,D\}$ complex.

The mass balance for the porphyrin and dendrimer species reads

$$C_P = [P] + \sum_{i=1}^{n} i \times [P_i,D] \qquad \text{(C.2)}$$

$$C_D = [D] + \sum_{i=1}^{n} [P_i,D] \qquad \text{(C.3)}$$

where C_P and C_D are the analytical concentrations of porphyrin and dendrimer ($D/P = C_D/C_P$). Using eq C.1 in expressions C.2 and C.3 and reorganizing the terms, we obtain

$$[P] = C_P \times \left(1 + \sum_{i=1}^{n} i \times \left(\prod_{j=1}^{i} K_{Aj}\right) \times [P]^{i-1}[D]^{i}\right)^{-1} \qquad \text{(C.4)}$$

$$[D] = C_D \times \left(1 + \sum_{i=1}^{n} \left(\prod_{j=1}^{i} K_{Aj}\right) \times [P]^{i}\right)^{-1} \qquad \text{(C.5)}$$

For generation 2.5, we assumed $n = 1$ and eqs C.4 and C.5 can be combined into a quadratic equation on [P] from which the solutions are easily extracted. On the other hand, for generation 4.5, it was assumed that $n = 4$ and numerical solutions from eqs C.4 and C.5 were obtained through an iterative procedure. The calculated values for [P] and [D] are introduced in eq C.1 to obtain the complete set of $\{[P_i,D], i = 1,n\}$. These values are then used in expression 4 to calculate the fraction of excitation light absorbed by each complex, f_i, and by its turn, these are used in expression 5 to obtain the average relative fluorescence quantum yield of the system, ϕ^0/ϕ.

References and Notes

(1) (a) Tomalia, D. A.; Baker, H.; Dewald, J.; Hall, M.; Kallos, G.; Martin, S.; Roeck, J.; Ryder, J.; Smith, P. *Polym. J.* **1985**, *17* (1), 117−132. (b) Tomalia, D. A.; Naylor, A. M.; Goddard, W. A., III. *Angew. Chem., Int. Ed. Engl.* **1990**, *29*, 138−175. (c) Bosman, A. W.; Janssen, H. M.; Meijer, E. W. *Chem. Rev.* **1999**, *99*, 1665−1688.

(2) Janssen, H. M.; Meijer, E. W. In *Synthesis of Polymers−Materials, Science and Technology Series*; Schüter, A. D., Ed.; Cahn, R. W., Haasen, P., Kramer, E. J., Series Eds.; Wiley-VCH: Weinheim, Germany, 1999; p 403.

(3) Kleinman, M. H.; Flory, J. H.; Tomalia, D. A.; Turro, N. J. *J. Phys. Chem. B* **2000**, *104* (48), 11472−11479.

(4) (a) Watkins, D. M.; Sayed-Sweet, Y.; Klimash, J. W.; Turro, N. J.; Tomalia, D. A. *Langmuir* **1997**, *13* (12), 3136−3141. (b) Wade, D. A.; Torres, P. A.; Tucker, S. A. *Anal. Chim. Acta* **1999**, *397*, 17−31. (c) Richter-Egger, D. L.; Li, H.; Tucker, S. A. *Appl. Spectrosc.* **2000**, *54* (8), 1151−

1156. (d) Richter-Egger, D. L.; Landry, J. C.; Tesfai, A.; Tucker, S. A. *J. Phys. Chem. A* **2001**, *105* (28), 6826−6833.

(5) (a) Jockush, S.; Turro, N. J.; Tomalia, D. A. *Macromolecules* **1995**, *28* (22), 7416−7418. (b) Ottaviani, M. F.; Turro, C.; Turro, N. J.; Bossman, S. H.; Tomalia, D. A. *J. Phys. Chem.* **1996**, *100* (32), 13667−13674. (c) Ottaviani, M. F.; Turro, N. J.; Jockush, S.; Tomalia, D. A. *J. Phys. Chem.* **1996**, *100* (32), 13675−13686. (d) Jockush, S.; Ramirez, J.; Sanghvi, K.; Nociti, R.; Turro, N. J.; Tomalia, D. A. *Macromolecules* **1999**, *32* (13), 4419−4423.

(6) (a) Paulo, P. M. R.; Costa, S. M. B. *Photochem. Photobiol. Sci.* **2003**, *2*, 597−604. (b) Paulo, P. M. R.; Gronheid, R.; De Schryver, F. C.; Costa, S. M. B. *Macromolecules* **2003**, *36* (24), 9135−9144.

(7) (a) Matos, M. S.; Hofkens, J.; Verheijen, W.; De Schryver, F. C.; Hecht, S.; Pollak, K. W.; Fréchet, J. M. J.; Forier, B.; Dehaen, W. *Macromolecules* **2000**, *33* (8), 2967−2973. (b) Jiang, D.-L.; Aida, T. *J. Am. Chem. Soc.* **1998**, *120* (42), 10895−10901. (c) Stapert, H. R.; Nishiyama, N.; Jiang, D.-L.; Aida, T.; Kataoka, K. *Langmuir* **2000**, *16* (21), 8182−8188. (d) Rajesh, C. S.; Capitosti, G. J.; Cramer, S. J.; Modarelli, D. A. *J. Phys. Chem. B* **2001**, *105* (42), 10175−10188.

(8) (a) Yeow, E. K.; Ghiggino, K. P.; Reek, J. N.; Crossley, M. J.; Bosman, A. W.; Schenning, A. P.; Meijer, E. W. *J. Phys. Chem. B* **2000**, *104* (12), 2596−2606. (b) Choi, M.-S.; Aida, T.; Yamazaki, T.; Yamazaki, I. *Angew. Chem., Int. Ed.* **2001**, *40* (17), 3194−3198. (c) Choi, M. S.; Aida, T.; Yamazaki, T.; Yamazaki, I. *Chem.*−*Eur. J.* **2002**, *8* (12), 2668−2678.

(9) (a) Bo, Z.; Zhang, L.; Wang, Z.; Zhang, X.; Shen, J. *Mater. Sci. Eng., C* **1999**, *10*, 165−170. (b) Sakamoto, M.; Ueno, A.; Mihara, H. *Chem.*−*Eur. J.* **2001**, *7* (11), 2449−2458.

(10) Naylor, A. M.; Goddard, W. A., III; Kiefer, G. E.; Tomalia, D. A. *J. Am. Chem. Soc.* **1989**, *111* (6), 2339−2341.

(11) (a) Moreno-Bondi, M. C.; Orellana, G.; Turro, N. J.; Tomalia, D. A. *Macromolecules* **1990**, *23* (3), 910−912. (b) Gopidas, K. R.; Leheny, A. R.; Caminati, G.; Turro, N. J.; Tomalia, D. A. *J. Am. Chem. Soc.* **1991**, *113* (19), 7335−7342.

(12) (a) Kalyanasundaram, K.; Neumann-Spallart, M. *J. Phys. Chem.* **1982**, *86* (26), 5163−5169. (b) Kalyanasundaram, K. *Inorg. Chem.* **1984**, *23* (16), 2453−2459. (c) Vergeldt, F. J.; Koehorst, R. B. M.; van Hoek, A.; Schaafsma, T. J. *J. Phys. Chem.* **1995**, *99* (13), 4397−4405.

(13) (a) Neri, B. P.; Wilson, G. S. *Anal. Chem.* **1972**, *44* (6), 1002−1009. (b) Langhus, D. L.; Wilson, G. S. *Anal. Chem.* **1979**, *51* (8), 1139−1144.

(14) (a) Kano, K.; Nakajima, T.; Hashimoto, S. *J. Phys. Chem.* **1987**, *91* (27), 6614−6619. (b) Kemnitz, K.; Sakaguchi, T. *Chem. Phys. Lett.* **1992**, *196* (5), 497−503. (c) Kano, K.; Minamizono, H.; Kitae, T.; Negi, S. *J. Phys. Chem. A* **1997**, *101* (34), 6118−6124.

(15) Reddi, E.; Ceccon, M.; Valduga, G.; Jori, G.; Bommer, J. C.; Elisei, F.; Latterini, L.; Mazzucato, U. *Photochem. Photobiol.* **2002**, *75* (5), 462−470 and references therein.

(16) Guliaev, A. B.; Leontis, N. B. *Biochemistry* **1999**, *38* (47), 15425−15437.

(17) Bos, M. A.; Werkhoven, T. M.; Kleijn, J. M. *Langmuir* **1996**, *12* (16), 3980−3985.

(18) (a) Chernia, Z.; Gill, D. *Langmuir* **1999**, *15* (5), 1625−1633. (b) Takagi, S.; Shimada, T.; Eguchi, M.; Yui, T.; Yoshida, H.; Tryk, D. A.; Inoue, H. *Langmuir* **2002**, *18* (6), 2265−2272.

(19) (a) Chen, X.; Li, L.; Liu, M. *Langmuir* **2002**, *18* (11), 4449−4454. (b) Viseu, M. I.; Gonçalves da Silva, A. M.; Antunes, P.; Costa, S. M. B. *Langmuir* **2002**, *18* (15), 5772−5781.

(20) Ottaviani, M. F.; Bossmann, S. H.; Turro, N. J.; Tomalia, D. A. *J. Am. Chem. Soc.* **1994**, *116* (2), 661−671.

(21) Press, W. H.; Teukolsky, S. A.; Vetterling, W. T.; Flennery, B. P. *Numerical Recipes in FORTRAN, the Art of Scientific Computing*, 2nd ed.; Cambridge University Press: New York, 1992; p 678.

(22) O'Connor, D. V.; Phillips, D. *Time-Correlated Single Photon Counting*; Academic Press: London, 1984; pp 43 and 158.

(23) Ferreira, J. A. B.; Coutinho, P. J. G.; Costa, S. M. B.; Martinho, J. M. G. *Chem. Phys.* **2000**, *262* (2, 3), 453−465.

(24) *Handbook of Mathematical Functions*; Abramowitz, M., Stegun, I. A., Eds.; Dover: New York, 1965; p 924.

(25) (a) Gaver, D. P., Jr. *Oper. Res.* **1966**, *14* (3), 444−459. (b) Stehfest, H., *Commun. ACM* **1970**, *13* (1), 47−49.

(26) (a) Gouterman, M. *J. Chem. Phys.* **1959**, *30* (5), 1139−1161. (b) Gouterman, M. In *The porphyrins*; Dolphin, D., Ed.; Academic Press: New York, 1978; Vol. 3, Chapter 1.

(27) (a) Fuoss, R. M.; Kraus, C. A., *J. Am. Chem. Soc.* **1933**, *55*, 1019−1028. (b) Fuoss, R. M. *J. Am. Chem. Soc.* **1958**, *80* (19), 5059−5061. (c) Fuoss, R. M. *J. Am. Chem. Soc.* **1978**, *100* (17), 5576−5577. (d) Chiorboli, C.; Indelli, M. T.; Scandola, M. A. R.; Scandola, F. *J. Phys. Chem.* **1988**, *92* (1), 156−163.

(28) The ϕ terms entering in the relative quantum yields, ϕ^0/ϕ, are calculated as $(\int I_{em}(\omega)\, d\omega) \times (1 - 10^{-OD})^{-1}$, where I_{em} is the emission spectra expressed as a function of the wavenumber, ω, and OD is the optical density at the excitation wavelength. Here, ϕ^0 stands for the quantum yield of TMPyP in aqueous solution without dendrimer (only the ratios ϕ^0/ϕ have physical significance, since I_{em}'s are in arbitrary units).

(29) Stechemesser, S.; Eimer, W. *Macromolecules* **1997**, *30* (7), 2204−2206.

(30) The hydrodynamic radii, R_H, of generations 2.5 and 4.5 PAMAM dendrimers in water were estimated to be 19.8 and 31.9 Å, respectively, from results of holographic relaxation spectroscopy (ref 29) for the full-generation PAMAM dendrimers in the same solvents by fitting the following scaling law: $R_H = a \times M_w{}^b$, where M_w is the molecular weight of the dendrimer and a and b are fitting parameters.

(31) Okutsu, T.; Ooyama, M.; Hiratsuka, H.; Tsuchiya, J.; Obi, K. *J. Phys. Chem. A* **2000**, *104* (2), 288−292.

(32) Gilbert, A.; Baggott, J. E. *Essentials of Molecular Photochemistry*; CRC Press: London, 1991.

(33) Lakowicz, J. R. *Principles of Fluorescence Spectroscopy*; Plenum Press: New York, 1983.

(34) Maiti, N. C.; Mazumdar, S.; Periasamy, N. *J. Phys. Chem.* **1995**, *99* (27), 10708−10715.

(35) Using the formalism developed in ref 36, it is possible to show that for a 45° angle between the absorption and emission dipoles (that corresponds to an r_0 value of 0.1) only out-of-plane rotations are effective to depolarize the emission of TMPyP, since both transition dipoles are in the plane of the molecule.

(36) Szabo, A. *J. Chem. Phys.* **1984**, *81* (1), 150−167.

(37) (a) Nisato, G.; Ivkov, R.; Amis, E. J. *Macromolecules* **1999**, *32* (18), 5895−5900. (b) Topp, A.; Bauer, B. J.; Tomalia, D. A.; Amis, E. J. *Macromolecules* **1999**, *32* (21), 7232−7237. (c) Nisato, G.; Ivkov, R.; Amis, E. J. *Macromolecules* **2000**, *33* (11), 4172−4176.

(38) Jones, G., II; Zhou, X.; Vullev, V. I. *Photochem. Photobiol. Sci.* **2003**, *2*, 1080−1087.

(39) (a) Kurzyński, M.; Palacz, K.; Chelminiak, P. *Proc. Natl. Acad. Sci. U.S.A.* **1998**, *95*, 11685−11690. (b) Kurzyński, M. *Physica A* **2000**, *285*, 29−47.

(40) Albery, W. J.; Bartlett, P. N.; Wilde, C. P.; Darwent, J. R. *J. Am. Chem. Soc.* **1985**, *107* (7), 1854−1858.

(41) (a) Levin, P. P.; Ferreira, L. F. V.; Costa, S. M. B.; Katalnikov, I. V. *Chem. Phys. Lett.* **1992**, *193* (6), 461−468. (b) Levin, P. P.; Ferreira, L. F. V.; Costa, S. M. B. *Langmuir* **1993**, *9* (4), 1001−1008. (c) Levin, P. P.; Costa, S. M. B.; Ferreira, L. F. V. *J. Phys. Chem.* **1995**, *99* (4), 1267−1275.

(42) Sikorski, M.; Krystkowiak, E.; Steer, R. P. *J. Photochem. Photobiol., A* **1998**, *117*, 1−16 and references therein.

(43) Green, N. J. *Chem. Phys. Lett.* **1984**, *107* (4, 5), 485−488.

(44) Flannery, M. R.; Mansky, E. J. *Chem. Phys.* **1989**, *132*, 115−136.

(45) These values were calculated assuming a radius of 7 Å for TMPyP and radii of 19.8 and 31.9 Å for PAMAM dendrimers of generations 2.5 and 4.5, respectively, as previously referred.[29,30]

(46) This reasoning holds up even if the dendrimer's effective charge due to counterion condensation (as it was explained) is used to calculate $|Z_{\pm} \cdot l_B|$, in which case values of 52 and 101 nm are obtained for generations 2.5 and 4.5, respectively.

(47) (a) Tachiya, M. *J. Chem. Phys.* **1978**, *69* (6), 2375−2376. (b) Sano, H.; Tachiya, M. *J. Chem. Phys.* **1979**, *71* (3), 1276−1282. (c) Tachiya, M. *Radiat. Phys. Chem.* **1983**, *21* (1, 2), 167−175.

(48) Murata, S.; Matsuzaki, S. Y.; Tachiya, M. *J. Phys. Chem.* **1995**, *99* (15), 5354−5358.

(49) Marcus, R. A.; Sutin, N. *Biochim. Biophys. Acta* **1985**, *811*, 265−322.

(50) (a) Berberan-Santos, M. N.; Martinho, J. M. G. *Chem. Phys. Lett.* **1991**, *178* (1), 1−8. (b) Berberan-Santos, M. N.; Martinho, J. M. G. *J. Chem. Phys.* **1991**, *95* (3), 1817−1824. (c) Berberan-Santos, M. N.; Martinho, J. M. G. *Chem. Phys.* **1992**, *164*, 259−269.

(51) In the present case, it was not necessary to consider the spectral emission density factors in combining the kinetic traces into a calculated decay (see ref 52), since the experimental decays were measured over a wavelength range that approximately includes the emission spectra of both species.

(52) Andriessen, R.; Boens, N.; Ameloot, M.; De Schryver, F. C. *J. Phys. Chem.* **1991**, *95* (5), 2047−2058.

(53) (a) Borkovec, M.; Koper, G. J. M. *Macromolecules* **1997**, *30* (7), 2151−2158. (b) Cakara, D.; Kleimann, J.; Borkovec, M. *Macromolecules* **2003**, *36* (11), 4201−4207.

(54) PPIs have aliphatic chain segments, which are slightly shorter than PAMAMs.

(55) van Duijvenbode, R. C.; Rajanayagam, A.; Koper, G. J. M.; Baars, M. W. P. L.; de Waal, B. F. M.; Meijer, E. W.; Borkovec, M. *Macromolecules* **2000**, *33* (1), 46−52.

(56) (a) Belloni, L. *Colloids Surf., A* **1998**, *140*, 227−243. (b) Belloni, L.; Drifford, M.; Turq, P. *Chem. Phys.* **1984**, *83*, 147−154.